PROCEEDINGS, 51st Workshop on Geothermal Reservoir Engineering
Stanford University, Stanford, California, February 9-11, 2026
SGP-TR-230

High-Temperature Reservoir Thermal Energy Storage for Grid Stability Enhancement

[1] Sai Liu, [2] Pin-Chun Cho, [1] Shuvajit Bhattacharya, [2] Erhan Kutanoglu

[1] HotRock Geothermal, Bureau of Economic Geology, The University of Texas at Austin, Austin, TX, USA

[2] Operations Research and Industrial Engineering Program, The University of Texas at Austin, Austin, TX, USA

sai.liu@beg.utexas.edu

Keywords: High-temperature thermal energy storage, Reservoir modeling, Heat recovery, Power system, Grid stability

ABSTRACT

High-temperature reservoir thermal energy storage (RTES) represents a promising approach to storing surplus renewable energy and waste heat in subsurface formations for later recovery, offering a reliable pathway toward enhanced grid stability. To store heat using high-temperature fluid, deep reservoirs with depths greater than 2 km are required for minimal heat loss. However, the mechanism controlling the efficiency of RTES and its value on grid stability remain unclear due to a lack of research and field demonstrations. To reveal this mechanism and achieve optimal heat storage performance for quantifiable grid stability improvement, this study presents an in-depth numerical analysis of the thermal behavior and storage performance of an open-loop RTES system. The effects of critical factors on the system's performance are analyzed, including the injection temperatures during heat storage and production, injection rates, storage and production schedule. Results show that a higher injection temperature during storage with a lower one during production yields the highest heat recovery. A higher hot fluid injection rate for storage and a lower cold fluid injection rate for production results in the lowest thermal drawdown during production, which is the most beneficial for power generation. To achieve both high production temperature and thermal power, a balanced combination of longer duration storage and production is recommended. Building on these findings, a power system modeling framework based on linearized AC optimal power flow (LPAC) is developed to represent the joint operation of RTES and the power grid. RTES simulation outputs are incorporated as input parameters in the LPAC model, influencing generation dispatch and allowing evaluation of grid stability under stressed operating conditions. Results indicate that RTES, with stronger heat production performance, provide greater grid stability benefits. This framework offers a structured and quantifiable approach to evaluate the operational benefits of RTES, with analysis indicating improvements in grid stability and reliability during stressed conditions.

1. INTRODUCTION

Underground thermal energy storage (UTES) systems represent a significant advancement in managing thermal energy, offering solutions for both high and low-temperature applications by temporarily storing heat or cold for later use. This temporary storage is crucial for mitigating the mismatch between energy supply and demand, especially for intermittent renewable energy sources, such as solar and wind. UTES systems leverage the low thermal conductivity and high heat capacity of surrounding rock mass to achieve additional energy efficiency benefits (Park et al., 2012). High-temperature reservoir thermal energy storage (RTES) stands out among different UTES technologies due to its capacity for storing thermal energy at elevated temperatures (Amiri et al., 2023). This capability enables the integration of both renewable and non-renewable heat sources into complex energy systems, particularly with storage temperatures exceeding 50 °C (Fleuchaus et al., 2020). The principle of RTES involves storing thermal energy within subsurface geologic reservoirs, specifically hot water, which can be produced later for power generation or direct-use applications like heating and cooling (Dobson et al., 2023). High-temperature RTES can become an indispensable component in achieving net-zero energy goals (Jin et al., 2022a). A significant advantage of high-temperature RTES over other UTES types is its suitability for higher temperature applications and its instrumental role in facilitating high flow rates within permeable formations (Guglielmetti et al., 2021). While low-temperature aquifer thermal energy storage systems are common, particularly for space heating and cooling in the 5 to 30 °C range (Drijver et al., 2011), high-temperature RTES can integrate diverse high-temperature heat sources for power generation (Fleuchaus et al., 2020).

The integration of renewable energy (RE), such as wind and solar power into the power grid presents significant challenges for grid stability (Kumar et al., 2024). These sources are intermittent and uncertain (as well as low capacity factor), as their power generation depends on variable weather conditions, which negatively impacts the stability of connected power systems (Cuong et al., 2024). The absence of inherent inertia in many renewable energy systems, such as wind generators, also contributes to frequency response issues and complex power system dynamics (Sowmiya et al., 2017). Grid stability encompasses various aspects, including frequency, voltage, and rotor angle stability, all of which can be affected by the fluctuating nature of renewable energy generation (Kumar et al., 2024). The increasing penetration of RE can lead to voltage instability concerns, particularly with inverter-based systems (Singh et al., 2024). Therefore, enhancing grid stability is paramount to ensure the reliable and secure operation of modern power systems with a high proportion of renewable energy.

High-temperature RTES can significantly enhance grid stability by addressing the intermittency and uncertainty of renewable energy generation (Jin et al., 2022b). By storing excess heat from renewable energy extraction systems, such as solar-thermal systems converting intermittent solar energy into heat, during periods of high heat extraction rates and low demand, and then releasing it when needed, RTES can balance the energy supply-demand mismatch. This helps stabilize the grid by ensuring a consistent energy supply, compensating for

variable output, and providing ancillary services (Rakib et al., 2024). Specifically, high-temperature RTES can play a crucial role in stabilizing the grid with increasing penetration of renewable energy generation (Jin et al., 2022b).

Previous study by Jin et al. (2022a) analyzed machine-learning-assisted computational frameworks to optimize RTES formation and thermal energy storage operational parameters. Dobson et al. (2023) reviewed technical challenges in moderate and high-temperature RTES, such as insufficient site characterization, scaling, corrosion, and thermal breakthrough, identifying proper design and operational practices to mitigate these risks. Regarding grid stability, research has focused on control strategies, including machine learning-driven approaches like Support Vector Regression (SVR) techniques, to regulate grid frequency and voltage (Kumar et al., 2024). Hybrid energy storage systems, including battery storage, pumped hydro storage, and compressed air storage (Zhang et al., 2025), have been proposed to improve the unstable power output responses of renewable energy microgrids (Du Plooy et al., 2017).

No published studies exist on the optimization of RTES in a power grid system yet. While studies acknowledge the potential of RTES for grid stability, there has been a lack of detailed analysis integrating RTES with power system modeling to quantitatively assess grid stability enhancement benefits of RTES. This study aims to address these critical gaps by presenting an in-depth numerical analysis of the performance of a high-temperature RTES system. The main objective is to reveal the mechanisms controlling RTES efficiency and its value in enhancing grid stability. This study has the following novelties: It investigates the mechanism controlling an RTES system's heat storage performance and integrates RTES with grid stability analysis. Also, it develops a power system modeling framework based on linearized AC optimal power flow model (LPAC) that explicitly incorporates RTES simulation outputs as input parameters. This framework enables a structured approach to evaluating the operational benefits of RTES, specifically quantifying improvements in grid stability under stressed conditions.

2. MODELING OF RESERVOIR THERMAL ENERGY STORAGE SYSTEM

2.1 Fundamentals of RTES

Our conceptual diagram of the RTES system includes a reservoir, its overlying and underlying rock (confining zones), a pair of cold and hot wells, a heat exchanger, a heat source, and a power block (Figure 1). During the heat storage process, hot fluid, with a fixed injection temperature and flow rate, is injected at the hot well's inlet and flows into the reservoir, during which the reservoir near the hot well is heated. Cold fluid produced at the cold well extracts heat from the heat source, and heated fluid is reinjected into the hot well. Both cold and hot wells are shut in at the end of heat storage. Later, when stored heat needs to be extracted, cold fluid is injected into the cold well and extracts heat from the reservoir that was heated during storage. Hot fluid then exits the hot well and flows into the power block for power generation, after which fluid that has cooled down is reinjected into the cold well for continued heat production. With RTES, excess heat from sources like renewables and industrial processes can be stored underground and then produced when needed for power generation, thus improving grid stability.

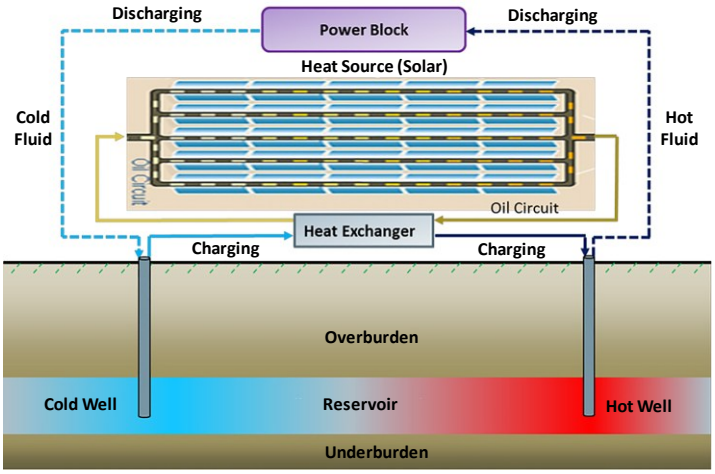

Figure 1: Diagram of reservoir thermal energy storage system (adapted from McTigue et al., 2023).

2.2 Physical and mathematical models

Main physical processes existing inside an RTES system involve fluid flow and heat transport among various components of the system. Our current RTES modeling does not incorporate geomechanics of the formation. Fluid flow in the well is assumed to be incompressible while following mass and moment conservation, respectively.

Heat is transmitted through multiple domains, including the rock formations, cement sheath, wellbore casing, and flowing fluid. The mathematical framework governing heat transfer is defined by a set of energy conservation equations. An energy conservation equation for porous media is used to characterize heat conduction and advection in the formation, formulated as (Liu and Taleghani, 2024; Liu et al., 2024)

$$(\rho C_p)_{eff}\frac{\partial T_r}{\partial t} + \rho_f C_{p,f}\mathbf{u}\nabla T_r - \nabla\cdot(\lambda_{eff}\nabla T_r) = 0, \quad (1)$$

where T_r is temperature in the formation; ρ_f is working fluid's density; $C_{p,f}$ stands for the specific heat capacity of working fluid; $(\rho C_p)_{eff}$ signifies the overall specific heat capacity of porous media, and λ_{eff} is the overall heat conductivity of porous media.

For incorporation of the injection temperature, T_{in}, the temperature at the intake is set to (Liu et al., 2023)

$$T|_{\Gamma} = T_{in}. \quad (2)$$

The temperature inside the whole system preceding fluid injection is formulated as

$$T|_{\mathrm{t=0}} = T_0(x, y, z), \quad (3)$$

in which T_0 signifies initial temperature, a function dependent on spatial coordinates. The governing equations above were solved using the finite difference method in computer modelling group (CMG) STARS (Liu and Bhattacharya, 2025). During heat production periods, thermal power achieved at the outlet of the hot well is calculated as (Liu and Taleghani, 2022, 2023)

$$P_{total} = \rho_{out}C_{out}\dot{V}_{out}T_{out} - \rho_{in}C_{in}\dot{V}_{in}T_{in}, \quad (4)$$

where $\rho_{in}C_{in}$ and $\rho_{out}C_{out}$ denote fluid heat capacities at the inlet and outlet, respectively; $\dot{V}_{in}$ and $\dot{V}_{out}$ denote fluid volumetric flow rates at the inlet and outlet, respectively; T_{in} and T_{out} are fluid temperatures at the inlet and outlet, respectively.

3. MODELING OF POWER GRID IN TEXAS

Given a set of candidate RTES operating locations, we use a linearized AC optimal power flow model (LPAC) to evaluate grid performance with RTES and compare the results to the baseline with no RTES. Specifically, 11 candidate RTES locations are identified based on major load centers and geothermal feasibility considerations, and these locations are treated as potential operating RTES sites in the evaluation model.

The test system is based on TX123-BT, a synthetic Texas grid mimicking the 2019 ERCOT grid, consisting of 123 buses, 255 transmission lines, and 292 generators distributed across major load centers and generation resources representative of the Texas grid (Lu et al., 2025). Figure 2 illustrates the TX123-BT topology and highlights the selected RTES operating locations. It is understood that current ERCOT grid structure (or what it will look like in the next 10 years) looks different than the synthetic grid we used in this study, but it serves the purpose to elucidate the role of RTES on grid resilience by simpler and time-efficient computations.

To assess the grid stability, the voltage stability index (VSI) and line stability index (LSI) are calculated. In our simulation, RTES is treated strictly as backup capacity, which means that it is dispatched only to support load shedding and is not used when the grid itself can satisfy the demand.

To represent a more stressed future operating environment with higher demand than that of the 2019 ERCOT grid, we use future climate data from the Electric Power Research Institute (EPRI), derived from quantile-shifted ERA 5 historical weather data (Smith et al., 2025). The dataset provides hourly weather profiles for 26 locations in Texas under future climate scenarios, SSP370, a high-emissions pathway. Under the SSP370 scenario, the projected profiles correspond to an average temperature increase of approximately 3.5°F, which is used to construct projected demand profiles that intentionally stress the grid to better distinguish how different RTES configurations influence grid performance.

Our evaluation focuses on the summer months, during which the grid is stressed to the point of requiring load shedding on an average of 8 days. During these stressed days, the grid experiences an average of 6 hours of load shedding duration, and RTES is dispatched to as backup capacity mainly to support the system during these time windows. In the remainder of this section, we introduce the equations, sets, parameters, and decision variables of the power grid model, and present the model formulation used in the simulation.

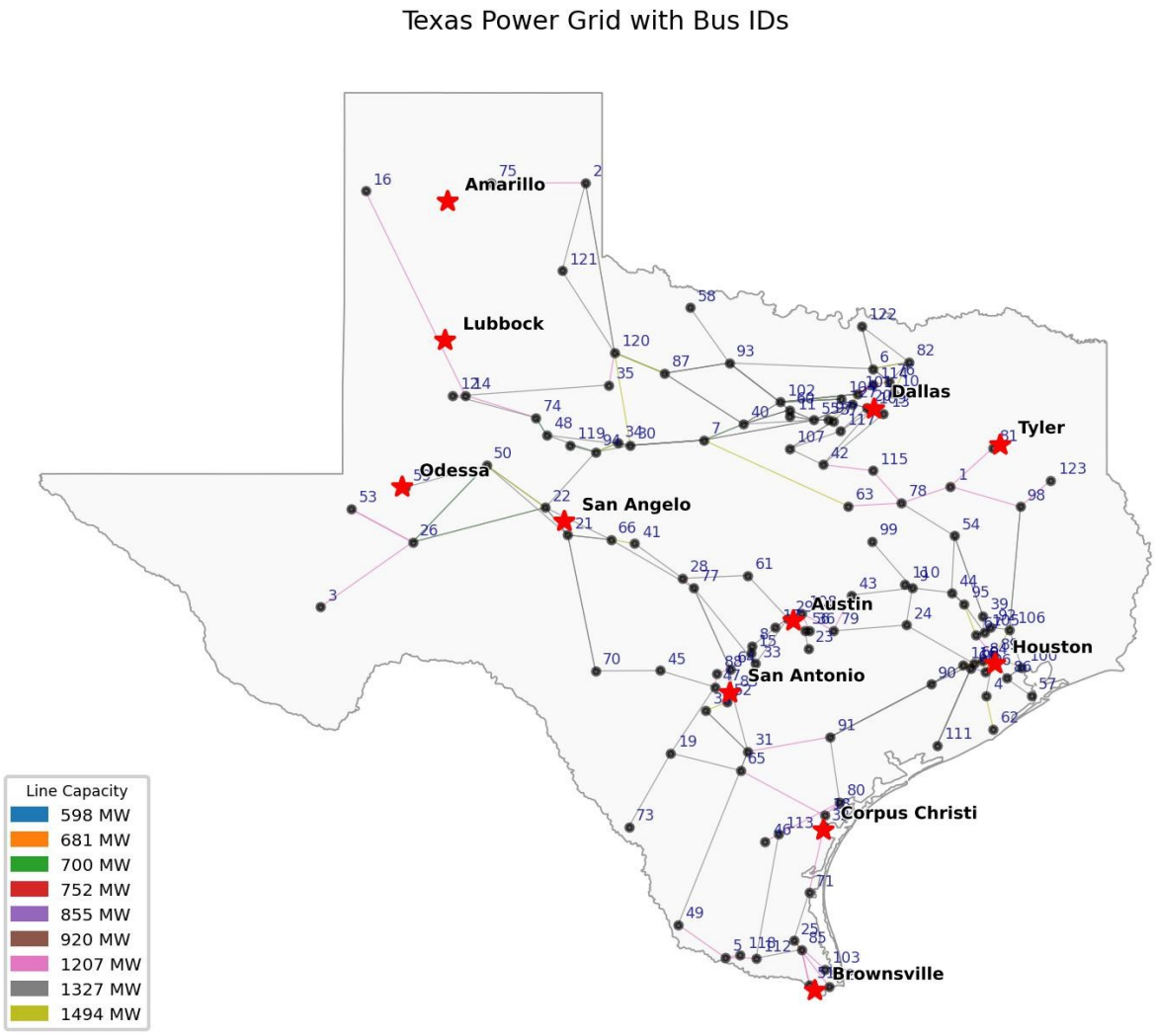

Figure 2: TX123-BT network topology (buses and transmission lines); star markers indicate 11 candidate RTES locations.

3.1 Notation

We present the notation used throughout the paper.

Sets

N: set of buses
G_n set of original generators at bus n
G_n^{TES} : set of RTES backup units are deployed at bus n
L: set of transmission lines (n, m)

K: set of time steps

Parameters

C_n, C_n^{RTES} marginal operational cost for active generation for original generators and RTES generators at bus n
$C^{loadshed}$: penalty cost per unit of unmet demand (load shedding)
$P_{n,k}^d, Q_{n,k}^d$: desired active and reactive load demand at bus n during time k
P_n^{gl}, P_n^{gu}: active generation lower and upper bounds at bus n
Q_n^{gl}, Q_n^{gu}: reactive generation lower and upper bounds at bus n
v^t: nominal operating voltage
v_n^l, v_n^u: voltage magnitude limits at bus n
$g_{nm,} b_{nm}$: calculated conductance and susceptance of the line (n.m)

$|V_n^t|$: target voltage magnitude at bus n, set to 1.0 p.u.
$\hat{P}_n^{RTES}$: maximum thermal power capacity of RTES at bus n, calculated by heat production from RTES
η: heat-to-electricity conversion efficiency
Decision Variables

$P_{n,k}^g, Q_{n,k}^g$: active and reactive generation at bus n during time k
$P_{n,k}^{RTES}, Q_{n,k}^{RTES}$: active and reactive generation for RTES backup units at bus n during time k
$l_{n,k}$: percentage of load served at bus n during time k where $l_{n,k} \in [0,1]$
$\theta_{n,k}$: voltage phase angle at bus n in radians
$\phi_{n,k}$: voltage magnitude deviation from the target $|V_n^t|$
cos_{nm} :linearized approximation of $\cos(\theta_n - \theta_m)$
p_l, q_l: active and reactive power flow across line l

3.2 Evaluation Model

Based on the above notations, we formulate an LPAC-based evaluation model that minimizes total operational cost while penalizing unmet demand, while only allowing RTES to provide backup support. The Warm-Start LPAC formulation follows the linearized AC power flow model in (Coffrin and Van Hentenryck, 2014).

In this model, RTES units are represented as additional dispatchable generators located at selected operating buses. To bridge the thermal components and the grid, the electrical output of the RTES at bus n is constrained by its maximum thermal capacity, $\hat{P}_n^{RTES}$, multiplied by heat-to-electricity conversion efficiency, η, which is set to 0.2. Assuming that RTES is only as backup capacity, its generation is allowed only to avoid load shedding. We enforce this restriction by assigning a significantly higher operational cost C_n^{RTES} to RTES compared to other generators, causing the model to prioritize existing generators and uses RTES only to support loadshed. The evaluation is modeled as:

$$\min \sum_k \sum_n \left(C_n P_{n,k}^g + C_n^{RTES} P_{n,k}^{RTES} + C^{loadshed} P_{n,k}^d (1 - l_{n,k}) \right) \quad (5)$$

s.t.

LPAC constraints

$$P_{n,k}^{RTES} \leq \eta \hat{P}_n^{RTES}, \qquad \forall n, k \quad (6)$$

The formulation is subject to two groups of constraints. The objective function, Equation (5), minimizes total hourly operational costs and loadshedding penalties across all time steps in the evaluation period. First, the Warm-Start LPAC constraints ensure nodal power balance and linearized AC power flow relationships to ensure feasible grid operation, details of which are omitted for brevity. Second, the RTES operational constraints model RTES production behavior. Constraint (6) ensures that the active power dispatch, $P_{n,k}^{RTES}$, is bounded by the electrical equivalent of the available thermal energy. With the outcomes from the evaluation model, we compute grid stability metrices to quantify and compare system performance across RTES cases.

3.3 Grid Stability Metrices (VSI and LSI)

To assess the impacts of RTES on grid stability, we compute the voltage stability index (VSI) and line stability index (LSI). Lower values of both indices indicate improved system stability and a greater buffer against potential voltage collapse or thermal overloads. (Salama and Vokony, 2022).

For each load bus n at time step k, VSI is computed as the absolute deviation from its 1.0 p.u. target magnitude. A smaller VSI shows that the bus voltage tends to be maintained near its target magnitude, reducing the risk of voltage instability. For each transmission line, LSI is computed as a function of the active power flow on line (n, m) at time k and the corresponding transfer limit from line parameters. A lower LSI suggests that a line has more room from its physical capacity limit. To obtain system-level indicators, VSI and LSI are averaged across all buses and transmission lines. These indices are further aggregated into annual averages and are used in Section 5 to assess grid stability. While steady-state stability is assessed in this study, future work might include frequency stability analyses to evaluate the role of RTES backup.

4. RESULTS FROM RTES ANALYSIS

Using the RTES simulation framework presented in Section 2, a baseline model was established first. The geometric parameters and boundary conditions of the baseline geologic model are in Table 1, and material properties are listed in Table 2. Using this baseline model, an analysis was conducted of the heat storage performances of the system under different operation conditions, including injection temperatures, injection rates, heat storage and production times. The outputs of RTES simulations were input into the grid modeling framework to evaluate quantitative grid stability improvements from RTES.

Table 1: Geometric parameters and boundary conditions of baseline RTES model.

Parameters	Units	Values	Parameters	Units	Values
Casing inner diameter	mm	271.32	Casing outer diameter	mm	298.45
Cement outer diameter	mm	374.65	Well depth	m	3000
Hot fluid injection rate during heat storage, $V_{in,s}$	m^3/d	3,000	Inlet temperature for storage, $T_{in,s}$	°C	200
Cold fluid injection rate during heat production, $V_{in,p}$	m^3/d	3,000	Inlet temperature for production, $T_{in,p}$	°C	40
Ambient temperature	°C	20	Geothermal gradient	°C/km	30
Reservoir thickness	m	100	Distance between cold and hot wells	m	200

Table 2: Subsurface geologic and engineering parameters adopted of baseline RTES model.

Parameters	Units	Overburden/ Underburden	Reservoir	Casing	Cement
Heat capacity	$J/(m^3 \cdot K)$	2.0×10^6	1.98×10^6	3.85×10^6	2.21×10^6
Thermal conductivity	W/(m·K)	1.1	2.4	45	1.3
Horizontal permeability (k_x, k_y)	mD	0.0001	100	-	-
Vertical permeability (k_z)	mD	0.0001	10	-	-
Porosity	p.u.	2	20	-	-

4.1 Effect of fluid injection temperatures

This section is aimed at exploring how the RTES system works at different injection temperatures. To this end, simulation was conducted of four cases with different injection temperature conditions, with $T_{in,s}$ and $T_{in,p}$ respectively denoting injection temperatures during heat storage and production. These cases were case 1: $T_{in,s} = 200$ ℃, $T_{in,p} = 20$ ℃; case 2: $T_{in,s} = 200$ ℃, $T_{in,p} = 40$ ℃; case 3: $T_{in,s} = 260$ ℃, $T_{in,p} = 20$ ℃; case 4: $T_{in,s} = 260$ ℃, $T_{in,p} = 40$ ℃. The highest $T_{in,s} = 260$ ℃ here was chosen by referring to Panja et al. (2021) that considered a hot fluid injection temperature of 250 ℃ during heat storage. For all cases, the operational procedure in each cycle (year) is as follows in time order: 3 months of heat storage, 3 months of well shut-in, 3 months of heat production, and 3 months of well shut-in. The total operation period is 10 years.

Figure 3a shows that $T_{in,s}$ has a more significant effect on production temperature than $T_{in,p}$. Specifically, at different times, production temperature grows as $T_{in,s}$ increases. For the same $T_{in,p} = 20$ ℃, as $T_{in,s}$ increases 200 ℃ from to 260 ℃, after-10-year production temperature improves to 212.52 ℃ by 43.76 ℃. At lower $T_{in,s} = 200$ ℃, increasing $T_{in,p}$ reduces production temperature slightly at the start of the first 4 cycles but improves it mildly thereafter. In comparison, as can be seen in Figure 3b, both $T_{in,s}$ and $T_{in,p}$ affect thermal power to a noticeable extent. At the same $T_{in,s}$, increase in $T_{in,p}$ impairs thermal power produced. Lower $T_{in,s}$ (200 ℃) and higher $T_{in,p}$ (40 ℃) in case 2 result in the smallest thermal power over time, while higher $T_{in,s}$ (260 ℃) and lower $T_{in,p}$ (20 ℃) in case 3 yield the highest power. Accordingly, case 3 achieves the largest 10-year cumulative heat production (6.28×10^5 MWh), which is 44.37% higher than the lowest value (4.35×10^5) obtained by case 2, as shown in Figure 4. As seen in Figure 5, when hotter fluid is injected during the heat storage phase, the formation temperature near the hot well is higher, which explains production temperature improvement brought by higher $T_{in,s}$.

In summary, the injection temperature during storage has much greater effect on production temperature than that during production. Injection temperatures in both phases influence thermal power noticeably. To achieve both high production temperature and cumulative heat production, the case of a higher injection temperature during storage and a lower one during production is recommended.

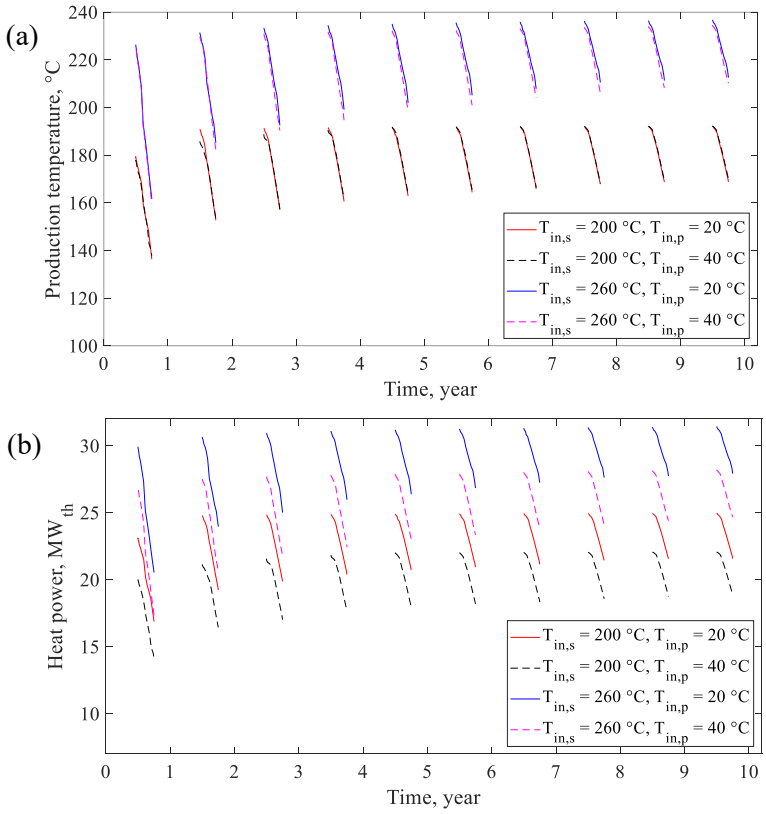

Figure 3: (a) Production temperatures and (b) thermal power versus time for different injection temperatures during heat storage and production ($T_{in,s}$: hot fluid injection temperature during heat storage, $T_{in,p}$: cold fluid injection temperature during production).

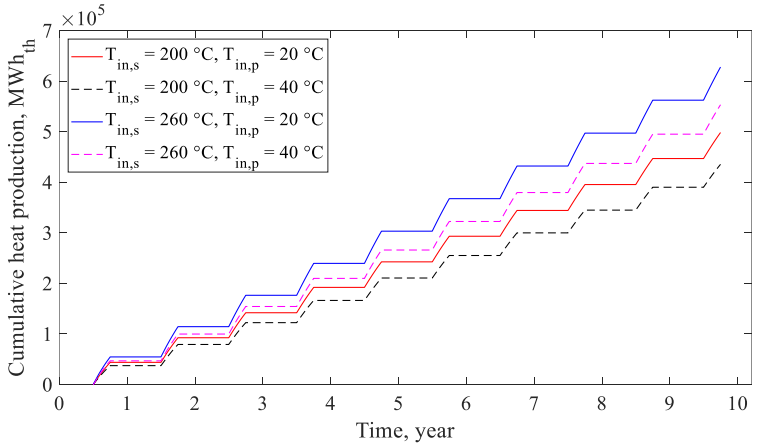

Figure 4: Cumulative heat production versus time for different injection temperatures during heat storage and production. In each year, cumulative heat production remains unchanged in the storage stage but increases during the production stage.

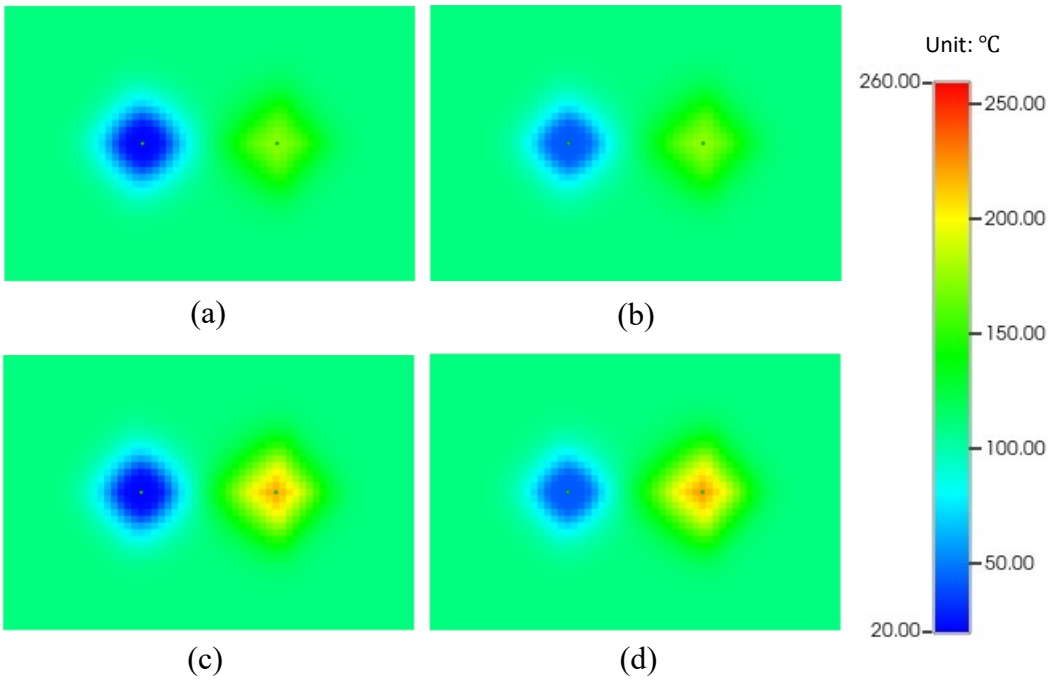

Figure 5: Plan views of after-10-year temperature distribution for different injection temperatures: (a) $T_{in,s} = 200$ ℃, $T_{in,p} = 20$ ℃; (b) $T_{in,s} = 200$ ℃, $T_{in,p} = 40$ ℃; (c) $T_{in,s} = 260$ ℃, $T_{in,p} = 20$ ℃; (d) $T_{in,s} = 260$ ℃, $T_{in,p} = 40$ ℃. The temperature surrounding the hot well is higher when hotter fluid is injected during heat storage.

4.2 Effect of fluid injection rates

To assess the effect of injection rates during storage and production on RTES performance, four cases with different injection rate combinations were simulated, including case 1: $V_{in,s} = 3000\ \mathrm{m^3/d}$, $V_{in,p} = 3000\ \mathrm{m^3/d}$; case 2: $V_{in,s} = 3000\ \mathrm{m^3/d}$, $V_{in,p} = 6000\ \mathrm{m^3/d}$; case 3: $V_{in,s} = 6000\ \mathrm{m^3/d}$, $V_{in,p} = 3000\ \mathrm{m^3/d}$; case 4: $V_{in,s} = 6000\ \mathrm{m^3/d}$, $V_{in,p} = 6000\ \mathrm{m^3/d}$. Here, $V_{in,s}$ and $V_{in,p}$ represent injection rates during heat storage and production, respectively. For all cases, the sequential injection and production events in each cycle (year) are the following: 3 months of heat storage, 3 months of well shut-in, 3 months of heat production, and 3 months of well shut-in. A total period of 10 years was simulated.

Figure 6 shows that in the first year, case 2 adopting lower $V_{in,s}$ and higher $V_{in,p}$ achieves the lowest production temperature, while case 3 using higher $V_{in,s}$ and lower $V_{in,p}$ yields the highest one. As time passes, case 4, which utilizes higher $V_{in,s}$ and $V_{in,p}$, yields higher production temperature than case 3 in the beginning of each cycle but falls below case 3 at the end of the cycle. After 10 years, the production temperature of case 3 is 192.76 ℃, which is the highest among all cases and 72.20 ℃ higher than the lowest obtained by case 2. In terms of thermal power, case 1 and case 4 respectively produce the smallest and largest values at any time. Figure 7 suggests that at different times, higher injection rates for storage and production in case 4 yield the largest cumulative heat production, while lower injection rates in case 1 result in the lowest. After 10 years, cumulative heat production (9.11×10^5 MWh) is achieved in case 4, 109.43% higher than that (4.35×10^5 MWh) in case 1. Figure 8 shows with lower $V_{in,s}$ and higher $V_{in,p}$ the temperature near the hot well is almost equal to initial reservoir temperature, indicating that stored heat has been completely extracted, explaining why this case yields the lowest production temperature and larger cumulative heat production than case 1 adopting lower $V_{in,s}$ and $V_{in,p}$. In case 3 where higher $V_{in,s}$ and lower $V_{in,p}$ are used, thermal interference is observed between cold and hot wells, and heat stored near the hot well is not efficiently extracted; this is why case 3 yields higher production temperature than case 4 in the end of each cycle but much lower thermal power.

To summarize, injection rates during storage and production significantly affect the performance of the RTES system. If the preference is extremely high production temperature, as in some power generation processes requiring high-temperature steam, a higher injection rate is suggested for storage and a lower one for production. In comparison, if both good production temperature and cumulative heat production are expected, a higher injection rate is recommended for both storage and production.

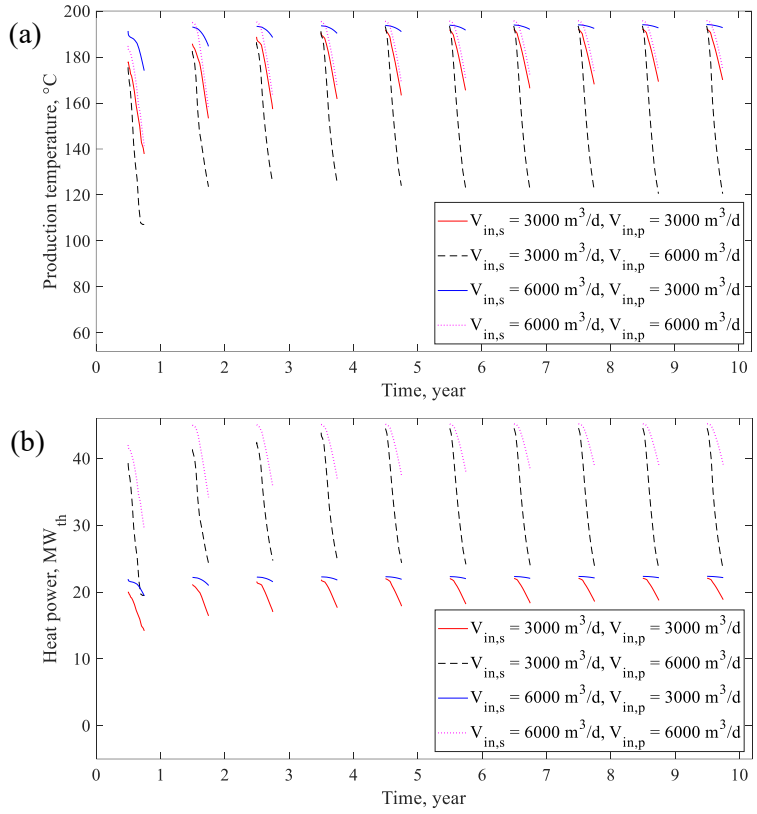

Figure 6: (a) Production temperatures and (b) thermal power versus time for different injection rates ($V_{in,s}$: hot fluid injection rate during heat storage, $V_{in,p}$: cold fluid injection rate during production).

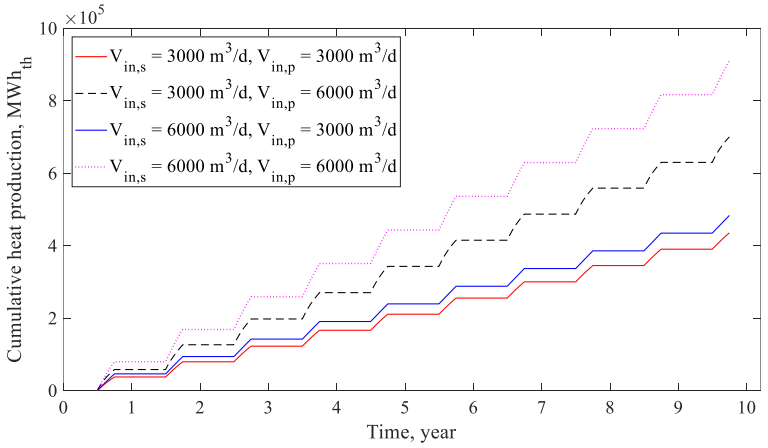

Figure 7: Cumulative heat production versus time for different injection rates during heat storage and production.

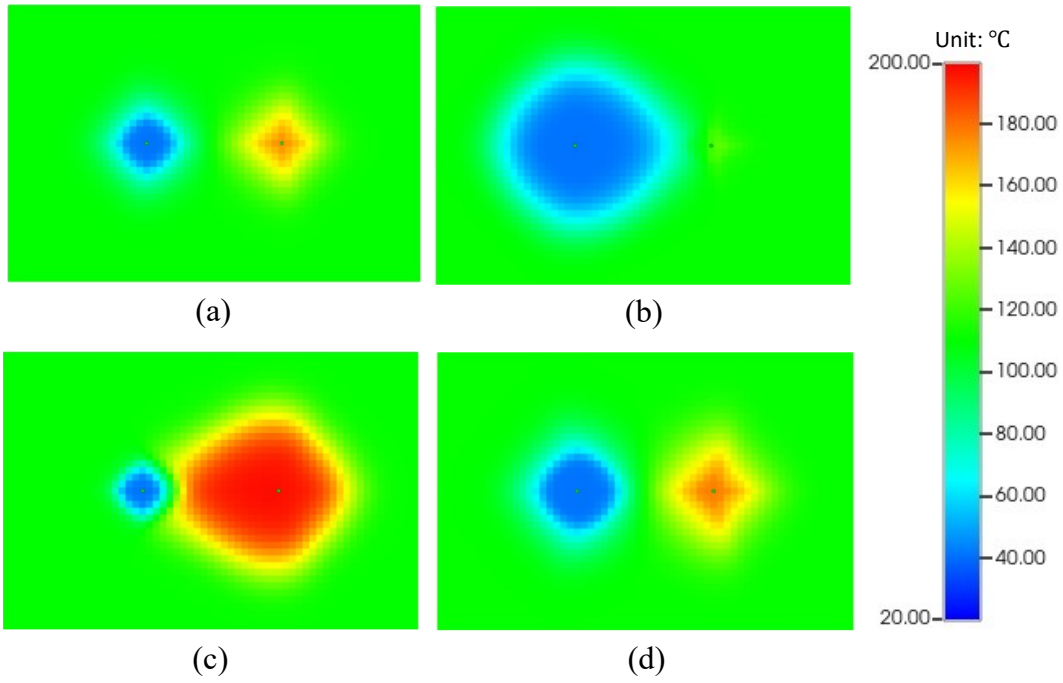

Figure 8: Plan views of after-10-year temperature distribution for different injection rates: (a) $V_{in,s}$ = 3000 m³/d, $V_{in,p}$ = 3000 m³/d; (b) $V_{in,s}$= 3000 m³/d, $V_{in,p}$ = 6000 m³/d; (c) $V_{in,s}$ = 6000 m³/d, $V_{in,p}$ = 3000 m³/d; (d) $V_{in,s}$ = 6000 m³/d, $V_{in,p}$ = 6000 m³/d.

4.3 Effect of heat storage and production times

Different scenarios of heat storage and production times are evaluated for the RTES system. In each cycle (year), the sequential injection and production events of each scenario are as follows:

case 1: 3 months of storage, 3 months of well shut-in, 3 months of production, and 3 months of well shut-in;

case 2: 3 months of storage and 9 months of production;

case 3: 6 months of storage and 6 months of production;

case 4: 9 months of storage and 3 months of production. A total period of 10 cycles is simulated.

Figure 9 shows that case 2 achieves the lowest long-term production temperature and thermal power at the end of each cycle, while case 4 yields the highest values, followed by case 3. This is because production duration in case 2 is much longer than storage time, causing heat stored near the hot well to be depleted and insufficient for production, as reflected by temperature distribution in Figure 11b. In contrast, heat storage duration is much longer than production duration in case 4, and heat stored is far more than enough for production, as confirmed by Figure 11d. Figure 11 also shows that there is significant temperature interference between cold and hot wells in cases 2 and 4, which also reduces the long-term production temperature of the system. Quantitatively, after a 10-year period, case 4 achieves a production temperature of 184.51 ℃, which is 88.95 ℃ higher than the one achieved by case 2. Figure 10 suggests that cases 2 and 3 lead to much higher cumulative heat production than cases 1 and 4 at different times.

Among different scenarios, case 3 obtains the highest 10-year cumulative heat production (8.98×10^5 MWh), which is 106.44% higher than the lowest value (4.35×10^5 MWh) yielded by case 1. Therefore, well shut-in leads to a lower performance of the system. Figure 9a also shows that the production temperature at the start of the first cycle of case 1 is slightly lower than that of case 2, which suggests that a shut-in period leads to slight heat loss from near the wellbore to far domains.

Storage and production times should be determined using the following strategy. If extremely high production temperature is preferred, as in special electricity generators requiring such high temperatures, a longer storage period and a shorter production period are recommended, but this leads to low heat recovery efficiency. However, if the objective is to achieve both satisfactory production temperature and cumulative heat production as well as high heat recovery efficiency, a balanced combination of storage and production times should be adopted without well shut-in periods, such as 6 months of storage and 6 months of production in each year.

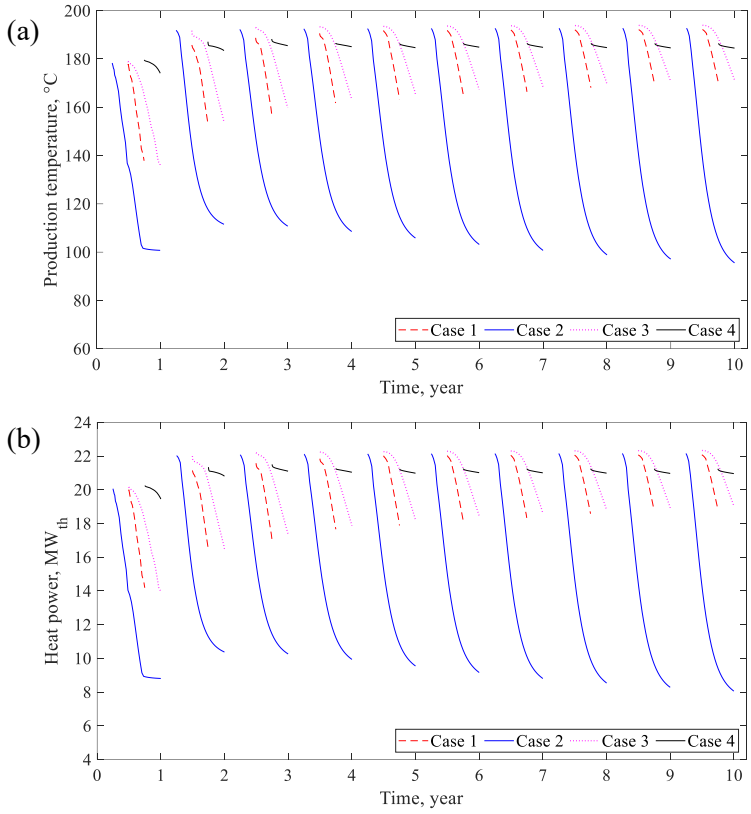

Figure 9: (a) Production temperatures and (b) thermal power versus time for different heat storage and production times. Case 1: 3 months of heat storage, 3 months of well shut-in, 3 months of heat production, and 3 months of well shut-in; case 2: 3 months of storage and 9 months of production; case 3: 6 months of storage and 6 months of production; case 4: 9 months of storage and 3 months of production.

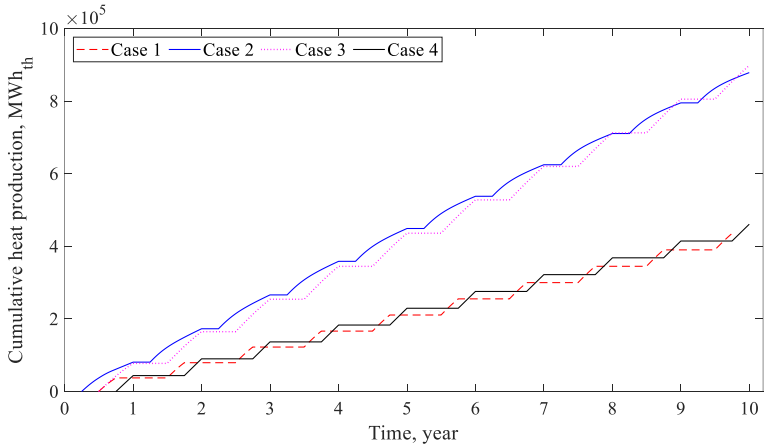

Figure 10: Cumulative heat production versus time for different heat storage and production times. Case 1: 3 months of heat storage, 3 months of well shut-in, 3 months of heat production, and 3 months of well shut-in; case 2: 3 months of storage and 9 months of production; case 3: 6 months of storage and 6 months of production; case 4: 9 months of storage and 3 months of production.

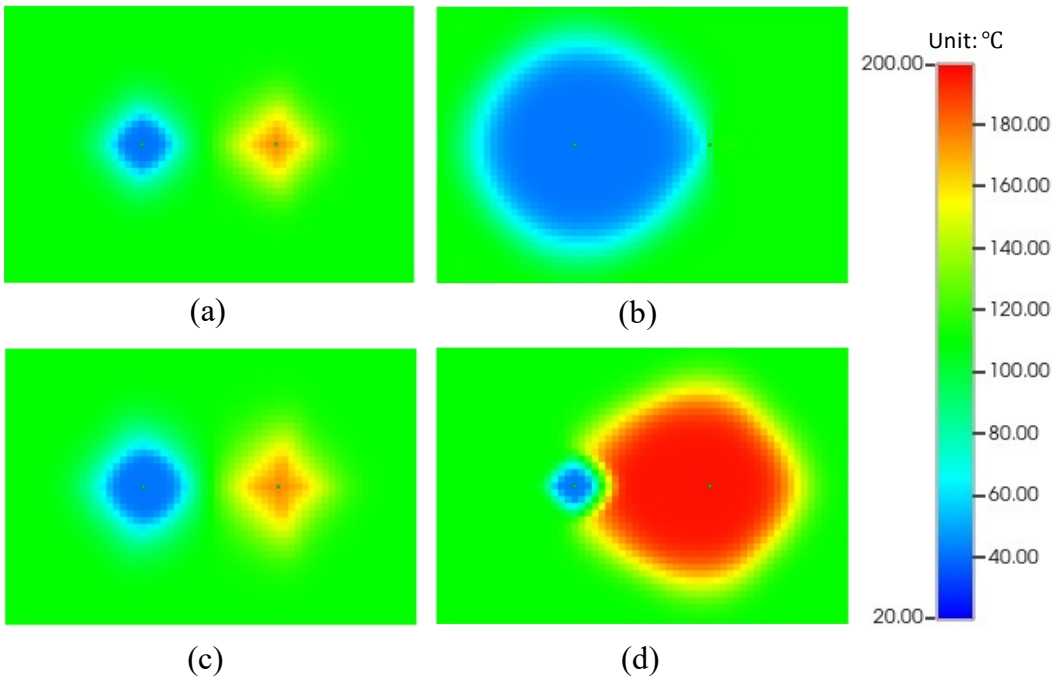

Figure 11: Plan views of after-10-year temperature distribution for different heat storage and production times: (a) case 1; (b) case 2; (c) case 3; (d) case 4. In both cases 2 and 4, temperature interference occurs between cold and hot wells, due to difference between storage and production times each year. case 1: 3 months of heat storage, 3 months of well shut-in, 3 months of heat production, and 3 months of well shut-in; case 2: 3 months of storage and 9 months of production; case 3: 6 months of storage and 6 months of production; case 4: 9 months of storage and 3 months of production.

5. RESULTS FROM GRID STABILITY ANALYSIS

To examine the performance of RTES in improving grid stability, numerical modeling was conducted to compare stability of a synthetic Texas power grid without and with RTES. The grid was evaluated over a three-year period (2019 – 2021). Hourly load and renewable profiles are generated by the projected weather data from 2019 to 2021. Because the demand levels in 2020 are lower in the input data, the grid operates under a comparatively less stressed condition in that year. As a result, the stability indices in 2020 are uniformly lower across all cases, independent of RTES settings (Figures 12 to 15).

The RTES performance was integrated into the grid model by mapping the heat production during the production time. Two groups of RTES scenarios were tested. The first group considers different TES injection rates, while the second group examines different heat storage and production times. This section presents the grid evaluation results for both groups.

5.1 Impact of RTES Injection Rates on Grid Stability

The RTES simulation results in section 4.2 were incorporated into grid modeling. The grid modeling results indicate that incorporating RTES consistently improves voltage stability. As shown in Figure 12, across all years, all RTES cases yield lower annual average VSI values compared to the no-RTES baseline, suggesting improved voltage stability under stressed conditions. Specifically, the two cases with lower heat production, the $V_{in,s} = 3000\ \mathrm{m^3/d}$, $V_{in,p} = 3000\ \mathrm{m^3/d}$ case and the $V_{in,s} = 6000\ \mathrm{m^3/d}$, $V_{in,p} = 3000\ \mathrm{m^3/d}$ case, still require load shedding, but the two cases with higher heat production, $V_{in,s} = 3000\ \mathrm{m^3/d}$, $V_{in,p} = 6000\ \mathrm{m^3/d}$ case and the $V_{in,s} = 6000\ \mathrm{m^3/d}$, $V_{in,p} = 6000\ \mathrm{m^3/d}$ case, provide sufficient backup support to maintain stability without the need for load shedding. Additionally, the observed stability improvement varies across RTES configurations and correlates with the RTES heat production performance reported in the previous section. Cases with stronger heat production performance provide greater backup capability and lead to more stability improvements. In particular, the $V_{in,s} = 6000\ \mathrm{m^3/d}$, $V_{in,p} = 6000\ \mathrm{m^3/d}$ case produces the lowest VSI among all four cases. Figure 13 shows the RTES reduces LSI mainly in the stronger heat production cases. Because the grid is stressed with high demand, lower heat production case may have limited ability to relieve line loading and thus have modest improvement. To summarize, higher flow rates can reduce the VSI and LSI, leading to improved grid stability. Table 3 shows the load shedding results for the injection rate scenarios across the three-year evaluation period. The results demonstrate that while the $V_{in,s} = 3000\ \mathrm{m^3/d}$, $V_{in,p} = 3000\ \mathrm{m^3/d}$ case and the $V_{in,s} = 6000\ \mathrm{m^3/d}$, $V_{in,p} = 3000\ \mathrm{m^3/d}$ case reduce outages, only the $V_{in,s} = 3000\ \mathrm{m^3/d}$, $V_{in,p} = 6000\ \mathrm{m^3/d}$ case and the $V_{in,s} = 6000\ \mathrm{m^3/d}$, $V_{in,p} = 6000\ \mathrm{m^3/d}$ case provide sufficient capacity to completely reduce load shedding across all tested years.

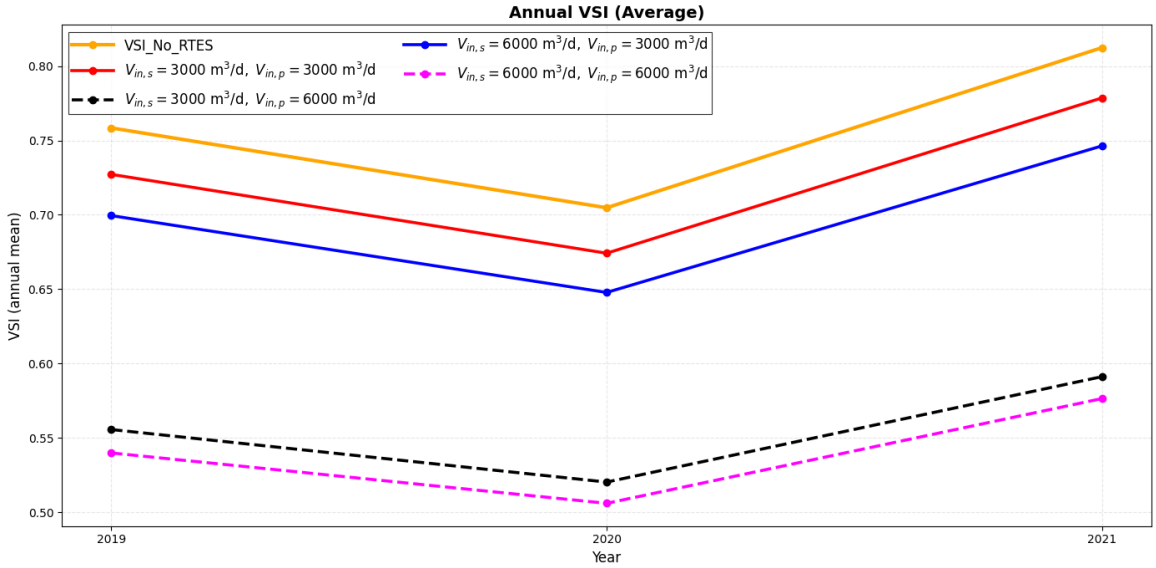

Figure 12: TX123-BT annual average VSI results for the no-RTES baseline and RTES injection-rate cases (2019-2021). After incorporating RTES, the VSI decreases, indicating improved grid stability. Because power demand is lower in 2020 than in 2019 and 2021, the VSI is lower in 2020 than in the other two years.

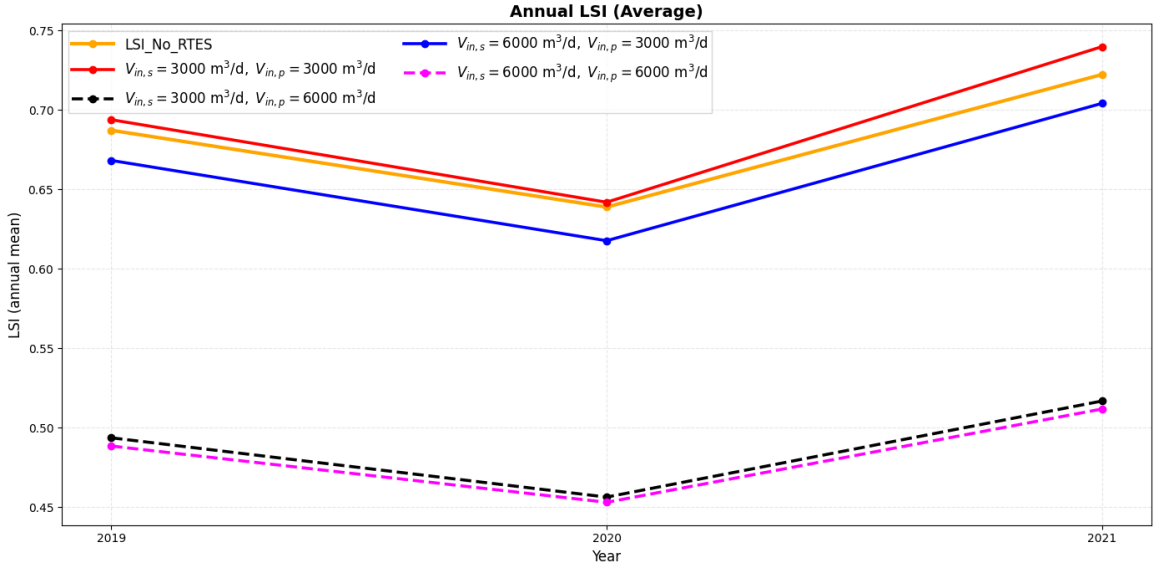

Figure 13: TX123-BT annual average LSI results for the no-RTES baseline and RTES injection-rate cases (2019-2021). After incorporating RTES, the LSI decreases, indicating improved grid stability. Because power demand is lower in 2020 than in 2019 and 2021, the LSI is lower in 2020 than in the other two years.

Table 3: Annual load shedding results for injection-rate scenarios (MWh). Note how RTES improves grid stability in the last two rows.

Scenario	**2019**	**2020**	**2021**
No RTES	3,579	2,793	5,124
$V_{in,s} = 3000\ \mathrm{m^3/d}, V_{in,p} = 3000\ \mathrm{m^3/d}$	2,963	2,066	4,323
$V_{in,s} = 6000\ \mathrm{m^3/d}, V_{in,p} = 3000\ \mathrm{m^3/d}$	2,662	1,902	3,910
$V_{in,s} = 3000\ \mathrm{m^3/d}, V_{in,p} = 6000\ \mathrm{m^3/d}$	0	0	0
$V_{in,s} = 6000\ \mathrm{m^3/d}, V_{in,p} = 6000\ \mathrm{m^3/d}$	0	0	0

5.2 Impact of RTES Heat Storage and Production Time on Grid Stability

The RTES simulation results in section 4.3 were incorporated into grid modeling. The grid modeling results indicate that RTES production scheduling also have an impact on grid stability performance. These cases evaluate how varying the duration of RTES production might affect the grid's ability to remain stable.

As shown in Figure 14, across all years, all RTES scheduling cases have lower annual average VSI compared to the no RTES baseline, indicating improved voltage stability. Compared to the results in Section 5.1, the differences in VSI improvements are relatively small since the four cases in this section have similar overall heat production rates. Nevertheless, slight variations can still be observed. Figure 15 demonstrates the LSI results. All RTES cases show reductions in LSI compared to the no RTES baseline, showing that RTES operations help reduce the line stress under the simulated grid conditions.

It is important to note that for all cases in this group, the grid still requires some load shedding under stressed conditions. However, the integration of RTES helps mitigate the stress compared to the baseline. Furthermore, the results suggest that RTES with a longer duration of storage, as seen in Case 3 and Case 4, can provide better support. Table 4 shows the load shedding results for the production time scenarios from 2019 to 2021. While load shedding occurs in all cases within this group, the data indicates that varying the storage and production scheduling impacts the frequency and magnitude of shedding events under stressed conditions.

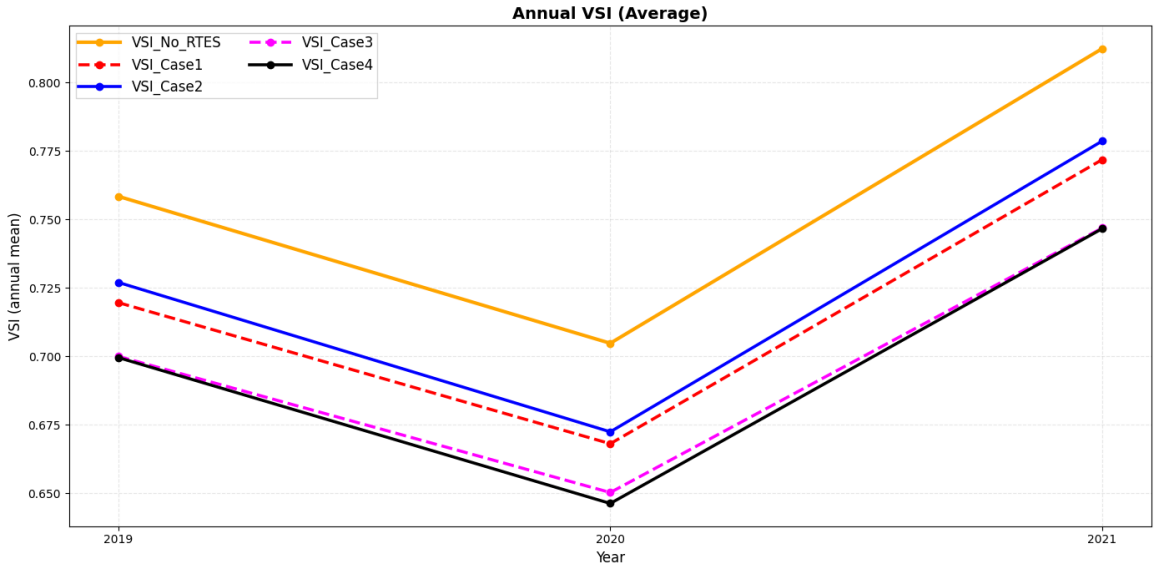

Figure 14: TX123-BT annual average VSI results for the no-RTES baseline and RTES production times cases (2019-2021). After incorporating RTES, the VSI decreases, indicating improved grid stability. Because power demand is lower in 2020 than in 2019 and 2021, the VSI is lower in 2020 than in the other two years.

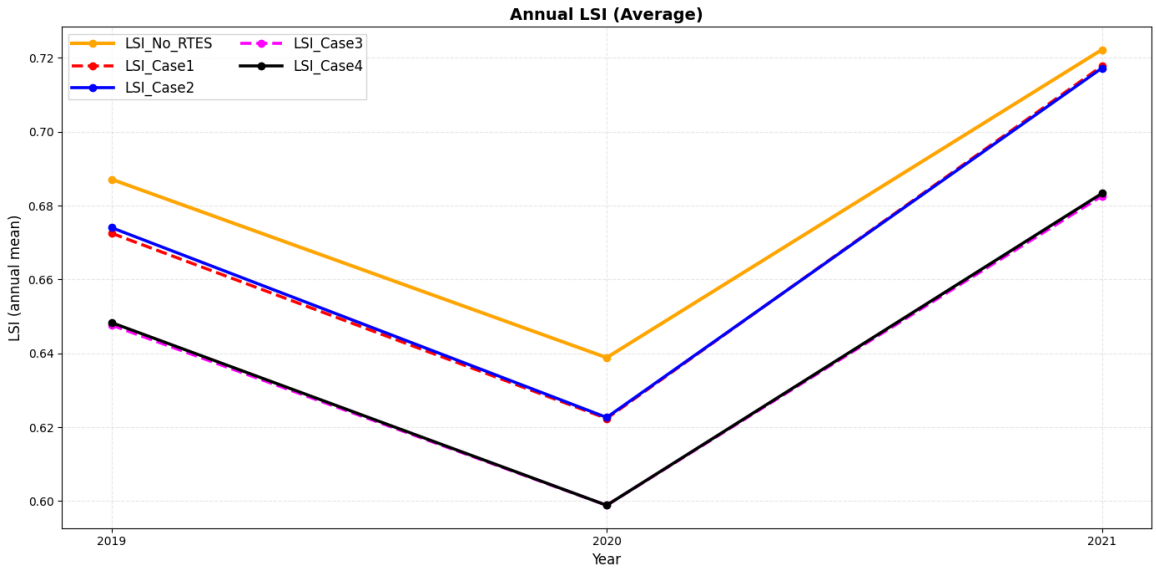

Figure 15: TX123-BT annual average LSI results for the no-RTES baseline and RTES production times cases (2019-2021). After incorporating RTES, the LSI decreases, indicating improved grid stability. Because power demand is lower in 2020 than in 2019 and 2021, the LSI is lower in 2020 than in the other two years.

Table 4: Annual load shedding results for production time scenarios. Note how RTES improves grid stability in various cases.

Scenario	2019	2020	2021
No RTES	3,579	2,793	5,124
Case 1	3,172	2,483	4,815
Case 2	3,342	2,617	4,812
Case 3	3,012	2,354	4,402
Case 4	2,902	2,221	4,213

6. CONCLUSIONS

In this paper, a high-temperature RTES is proposed as a solution to enhancing grid stability. A coupled thermo-hydraulic RTES system model is developed, based on which a systematic numerical study is performed to explore the system's performance under different operational conditions of injection temperatures, injection rates, and storage and production schedules. Principal findings are summarized as follows:

Hot fluid injection temperature during storage has a much more significant effect on production temperature than cold fluid injection temperature during production. At different times, production temperature grows as hot fluid injection temperature increases. To achieve both high production temperature and cumulative heat production, the case of a higher injection temperature during storage and a lower one during production is recommended.

Injection rates during storage and production phases significantly affect both the production temperature and thermal power of the RTES system. After 10 years of operation, the production temperature obtained with a higher hot fluid injection rate during storage and a lower cold fluid injection rate during production is the highest among all cases, 72.20 °C higher than the lowest achieved using a lower hot fluid injection rate and a higher cold fluid injection rate. The scenario of higher injection rates during both heat storage and production leads to the largest cumulative heat production, 9.11×10^5 MWh, 109.43% higher than the smallest acquired using lower injection rates.

At the end of each storage and production cycle, the case of shorter storage duration with longer production duration yields the lowest production temperature and thermal power, while longer storage duration with shorter production duration results in the highest values. Among various temporal schedules for storage and production, balanced storage and production duration without well shut-in yields the highest cumulative heat production, 8.98×105 MWh, which is 106.44% higher than the lowest achieved by the schedule incorporating shut-in.

The grid evaluation results show that using RTES as backup support improves both voltage and line stability under stressed operating conditions. Higher flow rates and longer storage duration can increase the heat production rate, which can reduce VSI and LSI, thereby increase grid stability. The extent of grid stability improvement correlates with RTES heat production performance, with higher heat production providing greater stability margins, minimizing voltage deviations and lowering the VSI. RTES improves line stability by supplying local power to critical load buses, which reduces transmission congestion and lowers the LSI.

While this study focuses on the summer peak stress scenarios, the findings suggest that its benefits can also be extended to extreme winter scenarios, such as Winter Storm Uri in 2021. In such scenarios, RTES and other subsurface storage technologies could serve as backup to stabilize the grid when traditional generators fail due to freezing conditions and underperform due to other reasons.

Because RTES improves both voltage and line stability, it offers a versatile solution for mitigating the impact of generator outages regardless of the season. In the future, advanced wellbore geometry and pressure storage, alongside winter-specific demand and potential generator outage profiles, are promising future research directions for grid stability enhancement.

REFERENCES

Amiri, L., Ermagan, H., Kurnia, J. C., Hassani, F., & Sasmito, A. P. (2024). Progress on rock thermal energy storage (RTES): A state of the art review. Energy Science & Engineering, 12(2), 410-437.

Coffrin, C., Van Hentenryck, P. (2014). A Linear-Programming Approximation of AC Power Flows. INFORMS Journal on Computing 26, 718–734.

Cuong, N. H., Tuan, T. Q., & Besanger, Y. (2024, October). Stability Analysis of Grid with High Renewable Energy Sources Under Uncertainty Conditions. In 2024 IEEE PES Innovative Smart Grid Technologies Europe (ISGT EUROPE) (pp. 1-5). IEEE.

Dobson, P. F., Atkinson, T. A., Jin, W., Acharya, M., Akindipe, D., Li, B., ... & Kumar, R. (2023, August). Hybrid uses of high-temperature reservoir thermal energy storage: lessons learned from previous projects. In SPE Energy Transition Symposium (p. D011S001R001). SPE.

Drijver, B., van Aarssen, M., & Zwart, B. D. (2012). High-temperature aquifer thermal energy storage (HT-ATES): sustainable and multi-usable. Proceedings of the Innostock, 1-10.

Du Plooy, H., Adonis, M., & Raji, A. (2017, April). The impact of energy storage on the stability of renewable energy in a micro grid. In 2017 International Conference on the Domestic Use of Energy (DUE) (pp. 173-178). IEEE.

Enescu, D., Chicco, G., Porumb, R., Seritan, G. (2020). Thermal Energy Storage for Grid Applications: Current Status and Emerging Trends. Energies 13.

Fleuchaus, P., Schüppler, S., Bloemendal, M., Guglielmetti, L., Opel, O., & Blum, P. (2020). Risk analysis of high-temperature aquifer thermal energy storage (HT-ATES). Renewable and Sustainable Energy Reviews, 133, 110153.

Guglielmetti, L., Daniilidis, A., Valley, B., et al. (2021). Screening of national potential for UTES, GEOTHERMICA – ERA NET Cofund Geothermal. European Union. https://www.heatstore.eu/documents/HEATSTORE_WP1_D1.3_Final_2021.10.28.pdf

Jin, W., Atkinson, T. A., Doughty, C., Neupane, G., Spycher, N., McLing, T. L., ... & Podgorney, R. (2022a). Machine-learning-assisted high-temperature reservoir thermal energy storage optimization. Renewable Energy, 197, 384-397.

Jin, W., Atkinson, T., Neupane, G., McLing, T., Doughty, C., Spycher, N., ... & Smith, R. (2022b). Influence of mechanical deformation and mineral dissolution/precipitation on reservoir thermal energy storage. In ARMA US Rock Mechanics/Geomechanics Symposium (pp. ARMA-2022). ARMA.

Kumar, P. P., Nuvvula, R. S., Shezan, S. A., Satyanarayana, V., SivaSubramanyamReddy, R., Ahammed, S. R., & Ali, A. (2024, May). Grid Stability Enhancement through Machine Learning-driven Control Strategies in Renewable Energy Integration. In 2024 12th International Conference on Smart Grid (icSmartGrid) (pp. 317-321). IEEE.

Liu, S., Al Balushi, F., & Taleghani, A. D. (2023). Heat extraction through conductive proppants. Sustainable Energy Technologies and Assessments, 60, 103514.

Liu, S., & Bhattacharya, S. (2025, October). Feasibility of Heat Production from Salt Domes Using Next-Generation Closed-Loop Geothermal Systems. In SPE Annual Technical Conference and Exhibition (p. D031S031R009). SPE.

Liu, S., & Taleghani, A. D. (2022). A Numerical Study of Factors Affecting the Efficiency of Closed-Loop Geothermal Wells. In 2022 Geothermal Rising Conference: Using the Earth to Save the Earth, GRC (pp. 160-172).

Liu, S., & Taleghani, A. D. (2023). Analysis of an enhanced closed-loop geothermal system. Geoenergy Science and Engineering, 231, 212296.

Liu, S., & Taleghani, A. D. (2024, September). Heat Extraction Through an Advanced Closed-Loop Geothermal System. In SPE Annual Technical Conference and Exhibition. (p. D011S006R003). SPE.

Liu, S., Taleghani, A. D., & Ji, K. (2024). An advanced closed-loop geothermal system to substantially enhance heat production. Energy Conversion and Management, 322, 119168.

Lu, J., Li, X., Li, H., Chegini, T., Gamarra, C., Yang, Y.C.E., Cook, M., Dillingham, G. (2025). A synthetic Texas power system with time-series weather-dependent spatiotemporal profiles. Sustainable Energy, Grids and Networks 43, 101774.

McTigue, J. D., Zhu, G., Akindipe, D., & Wendt, D. (2023). Geological Thermal Energy Storage Using Solar Thermal and Carnot Batteries: Techno-Economic Analysis (No. NREL/CP-5700-87000). National Renewable Energy Laboratory (NREL), Golden, CO (United States).

Panja, P., McLennan, J., & Green, S. (2021). Influence of permeability anisotropy and layering on geothermal battery energy storage. Geothermics, 90, 101998.

Park, D. Y., Kim, H. M., Ryu, D. W., Choi, B. H., SunWoo, C., & Han, K. C. (2012). Technologies of underground thermal energy storage (UTES) and Swedish case for hot water. Tunnel and Underground Space, 22(1), 1-11.

Rakib, M. W., Munna, A. H., Farooq, T., Boker, A., & He, M. (2024). Enhancing grid stability and sustainability: Energy-Storage-Based hybrid systems for seamless renewable integration. European Journal of Electrical Engineering and Computer Science, 8(3), 1-8.

Salama, H.S., Vokony, I., (2022). Voltage stability indices–A comparison and a review. Computers and Electrical Engineering 98, 107743.

Singh, P., Kumar, U., Choudhary, N. K., & Singh, N. (2024). Advancements in protection coordination of microgrids: A comprehensive review of protection challenges and mitigation schemes for grid stability. Protection and Control of Modern Power Systems, 9(6), 156-183.

Smith, E. T., Diaz, D. B., & Mardian, J. (2025). A Climate-Informed Approach to Create Hourly Future Weather Timeseries for Power System Planning. *IEEE Access*.

Sowmiya, A., Preethi, A., Priyaa, N.M. (2017). Enhancement of Grid Stability with A Possible Configuration of Motor-Generator Pair for Renewable Energy Integration. Bonfring International Journal of Power Systems and Integrated Circuits, 7, 3.

Zhang, Q., Taleghani, A. D., & Elsworth, D. (2025). Underground energy storage using abandoned oil & gas wells assisted by geothermal. Journal of Energy Storage, 110, 115317.